J Mol Model (2015) 21: 32
DOI 10.1007/s00894-015-2569-5

ORIGINAL PAPER

Anisotropy and roughness of the solid-liquid interface of BCC Fe

Yongli Sun · Yongquan Wu · Xiuming Lu · Rong Li · Junjiang Xiao

Received: 6 May 2014 / Accepted: 2 January 2015 / Published online: 31 January 2015

Abstract Melting point T_m and kinetic coefficient μ (a proportional constant between the interfacial velocity ν and undercooling ΔT), along with the structural roughness of the solid-liquid interface for body centered cubic (BCC) Fe were calculated by molecular dynamics (MD) simulation. All simulations applied the Sutton-Chen potential, and adopted average bond orientational order (ABOO) parameters together with Voronoi polyhedron method to characterize atomic structure and calculate atomic volume. Anisotropy of T_m was found through about 20~40 K decreasing from [100] to [110] and continuously to [111]. Anisotropy of μ with three low index orientations was found as: $\mu_{s,[100]} >> \mu_{s,[110]} > \mu_{s,[111]}$ for solidifying process and $\mu_{m,[100]} >> \mu_{m,[111]} > \mu_{m,[110]}$ for melting process. Slight asymmetry between melting and solidifying was discovered from that the ratios of μ_m/μ_s are all slightly larger than 1. To explain these, interfacial roughness R_{int} and area ratio S/S_0 (ratio of realistic interfacial area S and the ideal flat cross-sectional area S_0) were defined to verify the anisotropy of interfacial roughness under different supercoolings/superheatings. The results indicated interfacial roughness anisotropies were approximately [100]>[111]>[110]; the interface in melting process is rougher than that in solidifying process; asymmetry of interfacial roughness was larger when temperature deviation ΔT was larger. Anisotropy and asymmetry of interfacial roughness fitted the case of kinetic coefficient μ very well, which could give some explanations to the anisotropies of T_m and μ.

Y. Sun · Y. Wu (✉) · X. Lu · R. Li · J. Xiao
Shanghai Key Laboratory of Modern Metallurgy and Materials Processing, Shanghai University, Yanchang Road 149, Zhabei District Shanghai 200072, China
e-mail: yqwu@shu.edu.cn

Keywords Anisotropy · Interfacial roughness · Kinetic coefficient · Molecular dynamics simulation · Solid–liquid interface

Introduction

Melting point, denoted as T_m, and kinetic coefficient, denoted as μ, of solid-liquid (*s-l*) interface are known to be important thermodynamic and kinetic properties for metallic materials. Both properties are associated directly with the interfacial atomic behavior which is still difficult in most cases to be observed directly by experiments. However, the molecular dynamics (MD) simulation has contributed a lot to this atomic exploration of interface [1–3]. For T_m, there are several methods in MD simulation to calculate it. The first is a traditionally static searching strategy, with which we found the T_m of face centered cubic (FCC) Fe was 2550 K [4], very far from the experimental equilibrium melting point (1811.0 K) [5]. It is partly because this method neglects the hysteresis during heating or cooling process. Then, we applied another method of superheating-supercooling hysteresis [6] to deduce T_m from the maximum superheating (T_c^+) and supercooling (T_c^-) as $T_m = T_c^+ - \sqrt{T_c^+ T_c^-} + T_c^-$ [6]. Based on this theory, we can give a linear relationship between T_m and $N^{-1/3}$ [7], where N is atom number of an isolated nanoparticle. By extrapolating this relationship to $N^{-1/3} \rightarrow 0$, which means the system tends to infinity, we found T_m of bulk Fe was about 1833.3 K, which is closest to the theoretical melting point from MD simulation up to now. Shibuta et al. [8] set the pressure of a coexisting system of solid and liquid phases at 0 with NPH (constant number, pressure,and enthalpy) ensemble, and found the melting point of body centered cubic (BCC) Fe was 2400 K. Another coexisting phases method (CPM) was adopted in 1994 to calculate aluminum's

melting point by Morris et al. [9]. They connected a liquid and a solid phase together with NVE (constant number, volume, and energy) ensemble, and obtained a polynomial line $T_m = T_0 + \alpha P + \beta P^2$ [9] as the function of melting point with pressure. Based on the scheme of Morris et al. [9], Sun et al. [10] found the melting point of BCC Fe was 2358.7 K (by an embedded atom method, i.e., EAM, potential [11]), 2311.8 K (by a pair potential) and 1772.0 K (by another EAM potential [12]). In addition, they found the system size has some effect on the results. As an upgrade version of CPM, the interfacial velocity method (IVM) with NPT (constant number, pressure, and temperature) ensemble was used [13] to calculate T_m by fitting the relationship between interface moving velocity and the temperature. When the interface velocity comes to zero (the *s-l* interface is kept steady, the system does not solidify or melt), the temperature is derived as melting point T_m. Compared with other methods, CPM and IVM are more thermodynamically reasonable, and it provides a stable or dynamic *s-l* interface to be observed for the details of solid frontier.

In this paper, both CPM and IVM are used to calculate the melting point of BCC Fe with Sutton-Chen potential [14], and further to detect the structural and moving details of the *s-l* interface during solidifying and melting processes.

As another important property, kinetic coefficient μ, the proportional constant between the *s-l* interfacial velocity ν and supercooling (or superheating) ΔT, is defined to describe the solidifying (or melting) ability [10, 17]:

$$v = \mu(T - T_m) \tag{1}$$

The *s-l* interface moves with the velocity ν under the driving force of $\Delta T = T - T_m$, and the coefficient is μ. In 1982, to explore the kinetic coefficient, Broughton, Gilmer, and Jackson [15] (BGJ) proposed a collision-limited growth model denoted firstly by Turnbull through fitting the velocity and supercooling for [100] oriented *s-l* interfaces in the Lennard-Jones system. The BGJ model can describe the growth rate of solid phase as:

$$v \propto \widetilde{V} d \left(1 - e^{-\Delta G / k_B T}\right) \tag{2}$$

In this equation, denotes the thermal velocity [15, 16], d is interplanar spacing along the crystal orientation. The driving force for crystallization in this model is the difference of Gibbs free energy, ΔG, between bulk liquid and solid [10, 16], which comes originally from the undercooling ΔT. k_B is Boltzmann constant. Comparing Eq. (1) with Eq. (2), we find the kinetic coefficient should be proportional to the interplanar spacing d of different orientation in the same crystalline metal. With this theory, the kinetic coefficients of many metals have been estimated, especially FCC metals [1, 17, 10]. Hoyt and Asta [16] used an EAM potential to calculate the kinetic coefficients of Ag and Au. They found the ratio of $\mu_{[100]}/\mu_{[110]} \sim d_{[100]}/d_{[110]} = \sqrt{2}$, and this result agreed well with BGJ model. However, they also found $\mu_{[111]}$ was the smallest one among the three index orientations, while the BGJ model predicts that $\mu_{[111]}$ should be the largest one. Most previous research works found the similar kinetic contradiction for FCC metals [10, 18, 19]. To date, very few MD simulations were performed for BCC metals to calculate μ, especially for BCC Fe. Sun et al. [18], as the first work to discuss the kinetic anisotropy for a BCC Fe system, found the values of μ were 32.5±1.6 cm/(s·K), 24.6±1.4 cm/(s·K) and 25.6±2.0 cm/(s·K) for [100], [110] and [111] orientations respectively. In addition, they repeated those experiments with other pair and EAM potentials, and obtained similar results of $\mu_{[100]}/\mu_{[110]} \sim 1.35$ and $\mu_{[100]}/\mu_{[111]} \sim 1.35$. After that, interfacial mobility in Mo and V was reported in 2006 by Hoyt et al. [20] that $\mu_{[100]}$ is the largest for Mo and the growth rates are isotropic in three directions for V. In 2010, Watanabe et al. [21] also calculated the $\mu_{[100]}$ and $\mu_{[110]}$ of BCC Fe with Finnis-Sinclair (FS) potential [22], and found $\mu_{[100]} > \mu_{[110]}$.

Besides the focus on the interfacial thermodynamics and kinetics in most literature, few methods were used to explore the structural details of *s-l* interface. With the help of Z number density (the average atom number density along the direction normal to the interface, usually along the Z axis) and Z local ordering parameter (average coordinate number along the normal direction) [23, 24], the location and the width [25–27, 24] of the *s-l* interface can be roughly determined. However, those two Z-dependent parameters rely much on artificial factors to determine the start and end positions of the interface [2, 26, 24]. This will affect the precise determination of the interface structural anisotropy. In this paper, after calculating T_m and μ, we also addressed some works on these questions and analyzed the atomic roughness of *s-l* interface for the first time.

Methods

Classical MD simulations with NVE and NPT ensembles were performed with different orientations and sizes of BCC Fe systems. The Sutton-Chen potential was used to describe the atom interaction. It was created based on the empirical *N*-body potentials, which were developed by Finnis and Sinclair for the description of cohesion in metals. This potential can accurately predict the thermodynamic and transport properties of metals and was widely used to simulate the liquid-solid phase transitions of metals and alloys. Our previous works [4] [7, 28] on phase transition of bulk Fe in continuous heating and cooling processes, nucleation, and structural evolution have proved the validity of Sutton-Chen potential for the description of Fe. All our simulations were performed with DL_POLY 2.0 [29–31] software. The leapfrog method was

used to integrate the classical equations of motions with a time step of 2.0 fs. The Berendsen thermostat [32] was used to control temperature and pressure. Periodic boundary conditions were applied in all three directions.

Firstly, CPM was used to calculate T_m of BCC Fe. To begin the simulation, a system composed of a certain number of atoms in a periodic cell with perfect BCC symmetry (along the long axis, i.e., Z direction, is the destined crystalline orientation) was heated to 1800 K, a point near the estimated melting temperature, in order to achieve an approximately equilibrated initial configuration of solid state. Then, a liquid system was created by continuously heating this solid system to a high enough temperature (about 2800 K) to make sure it completely melted. After that, the liquid system was cooled down to 1800 K again but without crystallization. Finally, both solid and liquid systems were jointed together along the long crystal orientation, as shown in Fig. 1. It must be noted that all of the above simulations are under NPT ensemble.

We then relaxed the whole system still under NPT condition for 1000 time steps near the melting temperature to eliminate the surface gap and the distortion pressure caused by the mismatch between the two contacted surfaces. Using fully periodic boundary conditions, two interfaces were achieved between the solid and liquid parts in a single box. Hereto, a complete initial configuration with coexisting solid and liquid phases was built as close as possible to the equilibrium state. Next, the coexisting system was relaxed with NVE ensemble for 1600 ps separately at different temperatures ranging from 1600 K to 1900 K at 50 K intervals. During these equilibrating processes under NVE conditions, the pressure P_i and the equilibrating temperature T_i changed interdependently.

We chose three groups of samples, corresponding to [100], [110], and [111] orientations respectively; and for each group, we also chose three samples with different sizes. System size $(n_x \times n_y) \times n_z$ was defined as follows: n_x and n_y mean the numbers of atom layers along X and Y directions respectively. n_z is the number of spacing along Z axis, normal to the s-l interface. The parentheses represent the cross section. Taking [100] orientation with $(20\times30)\times80$ size for example, we set 20 layers in X direction, 30 layers in Y direction and 80 in Z. Note that 80 layers contain 40 solid layers and another 40 liquid 'layers', as the liquid part was originated from the solid state. Here, three different sizes (with different cross sectional areas or lengths along Z axis) were set in [100], [110], and [111] orientations respectively to investigate the system size effects. All the details about the samples are listed in Table 1.

To differentiate the state of each atom and calculate the atomic volume, we adopt average bond orientational order (ABOO) parameters [33] together with Voronoi polyhedron method (VP) [34, 28]. ABOO can identify the BCC, FCC, and hexagonal close packed (HCP) Fe atoms from amorphous Fe. Different from traditional BOO and ABOO methods, the scheme of ABOO+VP is used to identify the first shell neighbors of Fe atoms more precisely. The strong thermal oscillations produce some tiny Voronoi faces, corresponding to the second shell neighbors, which would significantly disturb the identification process. To get rid of this effect, we cut the tiny Voronoi faces off if the area of a Voronoi face is smaller than 0.5 Å^2, and disregard its corresponding particle as the first shell neighbors. Then, we could accurately determine the first shell neighbors and thus identify the crystalline or amorphous structures of Fe atoms more precisely.

Results and discussion

Melting point

As described in the Methods section, during the equilibrating processes under NVE conditions, P_i and T_i change dependently with each other. Fitting those data, a relationship between equilibrating pressure and temperature was obtained. Figure 2

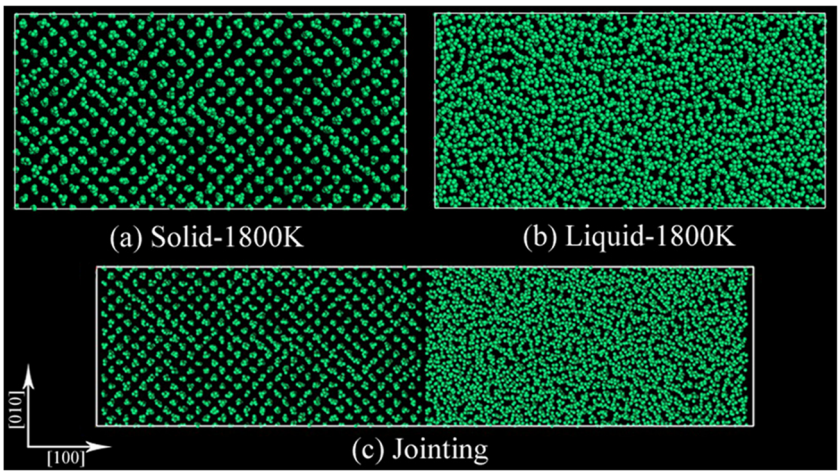

Fig. 1 Construction of the initial configuration of coexisting system by taking the [100] orientation as example (**a**) is the solid state at 1800 K by heating from the perfect BCC crystal at ambient temperature; (**b**) is the liquid state at 1800 K by cooling from completely molten state; (**c**) is the joint system of the above two systems. All above simulations were performed under NPT conditions

Table 1 Values of the melting points T_ms and kinetic coefficients μs calculated for various system orientations and sizes, along with the details of chosen samples. The notation for system size is described in the text. Previous works (T_ms derived from different methods, potentials for crystalline structures and μs for Fe by EAM potential) were listed for comparisons

Orientation	Size $((n_x \times n_y) \times n_z)$	Number of atoms	T_m (K)				μ (cm/(s·K))			
			CPM	IVM	Reference works		μ_s	μ_m	μ_m/μ_s	Reference results
[100]	(20×20)×80	8,000	1756.0	1752.5	1811.0	BCC [a] BCC [b]	56.66±2.00	58.86±2.43	1.04 1.45	45.8±3.8 [b] 30.5 [e]
	(20×30)×80	12,000	1753.6	1760.7	1772.0		63.18±1.78	91.57±3.60	1.26	
	(20×20)×120	12,000	1753.5	1755.6			58.43±1.35	73.50±2.55		
[110]	(20×20)×40	8,000	1718.0	1717.2	2251.0	FCC [b] BCC [c]	31.23±2.41	35.07±1.56	1.12	33.5±1.0 [b] 25.7 [e]
	(20×20)×60	12,000	1724.8	1720.3	2231.8		29.17±1.34	31.72±1.42	1.09	
	(20×20)×80	16,000	1734.6	1727.5			33.58±1.99	39.90±2.17	1.19	
[111]	(24×16)×84	8,064	1696.1	1691.6	2202.0	FCC [c] BCC [d]	26.64±1.34	28.89±1.37	1.08	31.8±1.8 [b]
	(30×20)×80	12,000	1702.8	1704.0	2400.0		31.24±1.08	55.17±3.16	1.77	
	(30×20)×132	19,800	1705.3	1705.6			23.55±0.35	33.98±0.91	1.44	

[a] Experimental [5]; [b] CPM method with EAM potential [18]; [c] CPM method with pair potential [18]; [d] NPH method with FS potential [35]; [e] FS potential [21]

shows this relationship for the systems of 12,000 atoms as an example. Thus, the thermodynamically equilibrated melting points at atmospheric pressure were obtained through the intersecting points between the fitting lines and the level line of 0.001 kbar. Through this analysis process, all T_ms from CPM were obtained and listed in Table 1.

The results of T_ms in Table 1 range from 1696 K to 1756 K, which are close to the experimental value (1811.0 K) [5], and are better than most previous works [18, 35]. Then, we can find that except for the [110] orientation, the system size has little effect on T_m, at least in the range of the system size in this paper. Note that, there's no sign showing that any distortion pressure, coming from the artificial surface cleaving and layer building process, exists to affect T_m after the NPT ensemble relaxation. We also found the computed T_ms show a certain differences among different orientations. For [100] orientation, T_m=1753~1756 K, while, for [110] and [111] the T_ms decrease down to 1718~1734.6 K and 1696~1705 K, respectively. The decreasing amplitudes are about 20~40 K from [100] to [110] and continuously to [111]. Sun et al. [10] also found the difference of T_ms in different orientations of FCC Ni, $T_{m,[100]}$=1712.6~1714.4 K, $T_{m,[110]}$=1701.1 K and $T_{m,[111]}$=1707.6~1720.1 K, about 20 K max variations with crystalline orientations. However, they found the system size in their calculation works on T_m. Sorkin et al. [36] simulated BCC V and found $T_{m,[111]}$=2220±10 K and $T_{m,[110]}$=2240±10 K. They also found that (111) surface disorders first, then (100) surface, while the (110) surface remains stable up to the melting temperature T_m. All these T_m anisotropies are similar to our results except that $T_{m,[100]}$s in our works are largest.

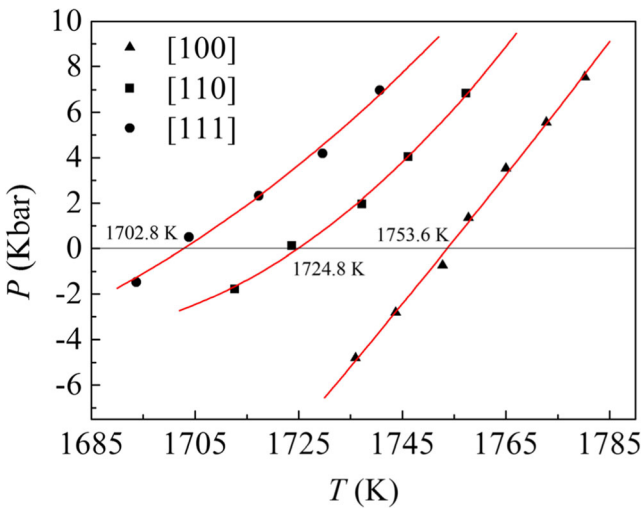

Fig. 2 The relationship between pressure P and temperature T of the coexisting systems consisting of 12,000 atoms for [100], [110], and [111] orientations under NVE ensemble. Temperatures indicated at 0.001 kbar are achieved as the equilibrium melting points at atmospheric pressure

Kinetic coefficient

As the continuous work, we use the coexisting system equilibrated at 1750 K as initial configuration and vary the system temperature from 1625 K to 1850 K at 25 K intervals to run 120,000 time steps (240 ps) separately. These simulations were all carried out with NPT ensemble. The pressure was fixed at 0.001 kbar. Figure 3 shows the snapshots of the three oriented systems after 35 ps, 50 ps, and 70 ps running at various temperatures. At temperature higher than T_m the solid phase melted, and the interface moved toward the solid side. On the contrary, when temperature was lower than T_m, the liquid field shrank, corresponding to the directional crystallization. Furthermore, as the supercooling or superheating got larger, the interface moved faster. It seems that the [110] and [111] orientations need more time to obtain the same solidification fraction as the [100] orientation.

Figure 4 is the time dependence of the system volumes for three orientations composed of 12,000, 12,000, and 19,800

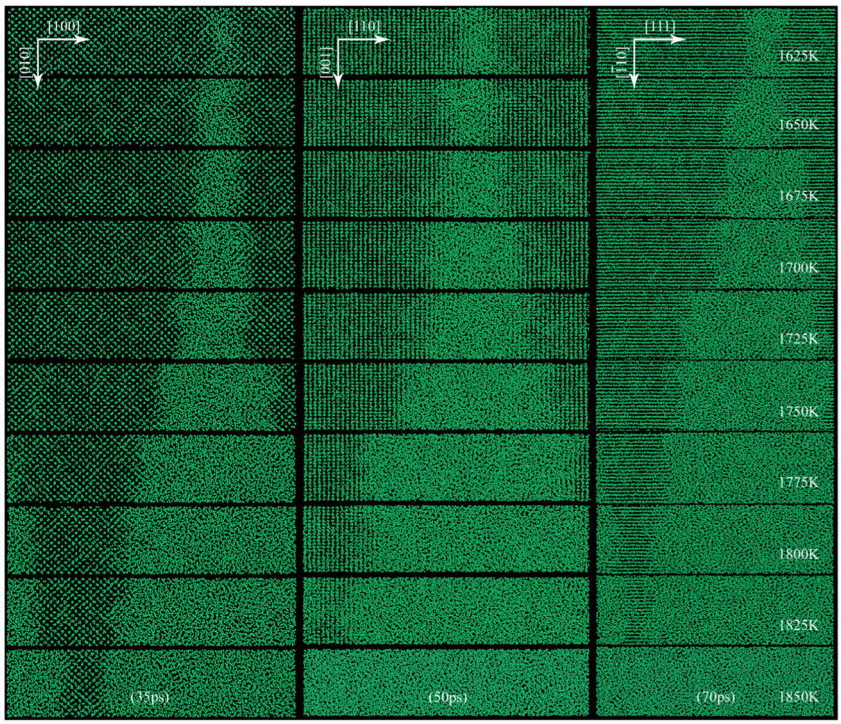

Fig. 3 The snapshots of systems along three directions after 35 ps, 50 ps, and 70 ps running in different temperatures ranging from 1625 K to 1850 K at 25 K intervals, starting from a same equilibrium state at 1750 K

atoms respectively. At temperature higher than T_m, the volume increased and on the contrary the volume decreased with time. The farther the temperature departs from T_m, the faster the volume changes. At the temperatures far from T_m, some platforms appear to indicate the whole system completely melted or crystallized.

From Fig. 4, the volumes of bulk solid and liquid phases, and the interfacial velocities v can be readily extracted [26, 17]. Once the slope of volume versus time, denoted as Ω, under different temperature is obtained, the v can be given as:

$$v(\Delta T) = \frac{\Omega d}{2n(\omega_l - \omega_s)} \tag{3}$$

where ω_l and ω_s denote volumes per atom for solid and liquid phase, respectively. The number 2 in denominator stands for the presence of two interfaces in the periodic simulation cell. d and n denote the interplanar spacing and the number of atoms per layer in the growth planar of the crystal, respectively.

With the atom identifying and volume calculating tools (ABOO+VP) described above, we can calculate the real-time volume of each atom, ω_l and ω_s, interplanar spacing d along Z axis and the number of atoms n per layer. Therefore, the interface moving velocity can then be directly calculated from Eq. (3) based on the achieved Ωs from Fig. 4. Figure 5 is the calculated real-time velocities of *s-l* interfaces corresponding to the three systems in Fig. 4. The insets are the relationships between velocities and ΔTs, and the linear fitting slope is the kinetic coefficient μ. To simplify the description, we name supercooling and superheating unifiedly as temperature deviation, ΔT; and according to the traditional definition, supercooling is set to be positive.

As described above, the *s-l* interface at T_m will shift neither to the solid side nor to the liquid side. So, T_m was obtained through fitting the linear relationship between interfacial velocity and temperature, and also listed in Table 1 to compare with CPM results. Note that, we fitted the positive and negative data with two independent linear functions under the condition of the same x intercept, i.e., T_m, according to the asymmetries of velocities between melting and solidifying found previously in many works [37, 19]. Asymmetry is the phenomenon that interfacial velocities are different between melting and solidifying with the same absolute value of ΔT. Melting is a disordering process above T_m, while, solidifying is an ordering stage below T_m. It is obviously harder to be crystallized at a lower temperature than to be melted at a higher temperature, especially when the crystal surface is not easy for liquid atoms to land on (see below). Previously, most of the results (T_m and μ) were obtained directly by fitting the positive and negative data with one single linear function, or just fitting positive data [35, 21]. This is inappropriate for asymmetric systems. Here, we use two linear functions to fit the positive and negative data points, respectively. As an important limiting condition, these two fitting lines have the same x intercept, which is the final determined T_m. These T_ms from IVM are listed next to CPM results in Table 1. The values of IVM results fit CPM results well despite some acceptable slight deviations (<7 K). Previous IVM results

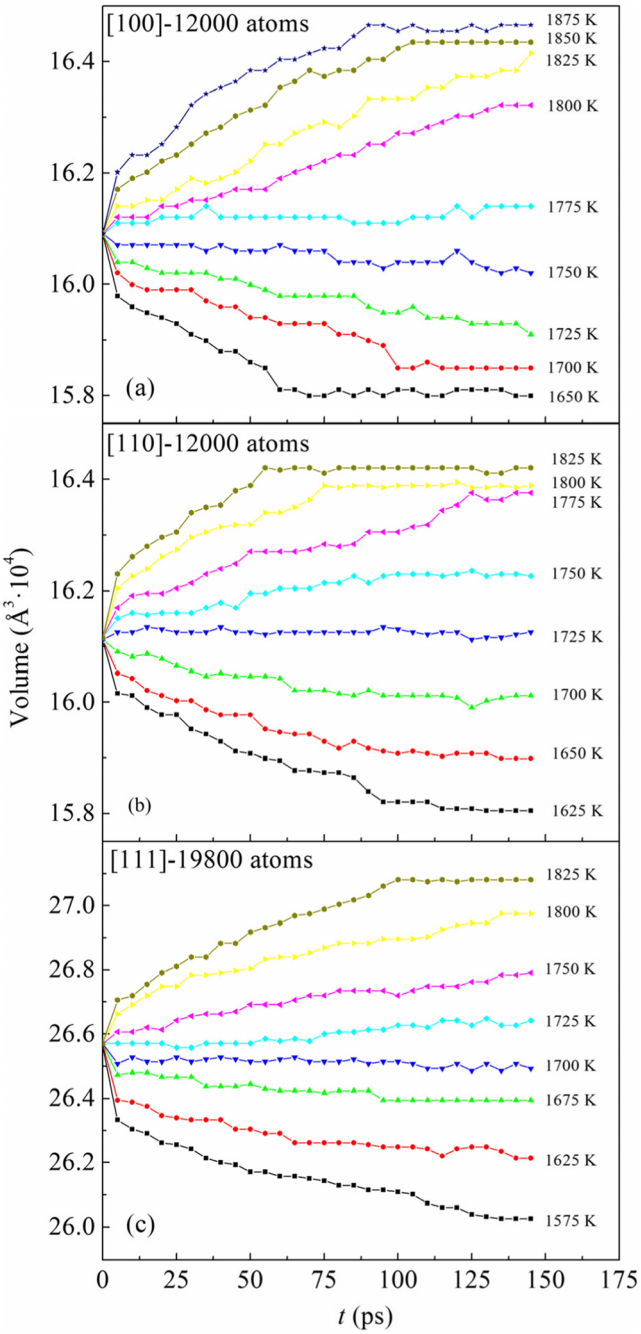

Fig. 4 Time dependence of the system volumes during solidifying/melting processes for the systems of [100], [110], and [111] orientations containing 12,000, 12,000, and 19,800 atoms respectively at different temperatures

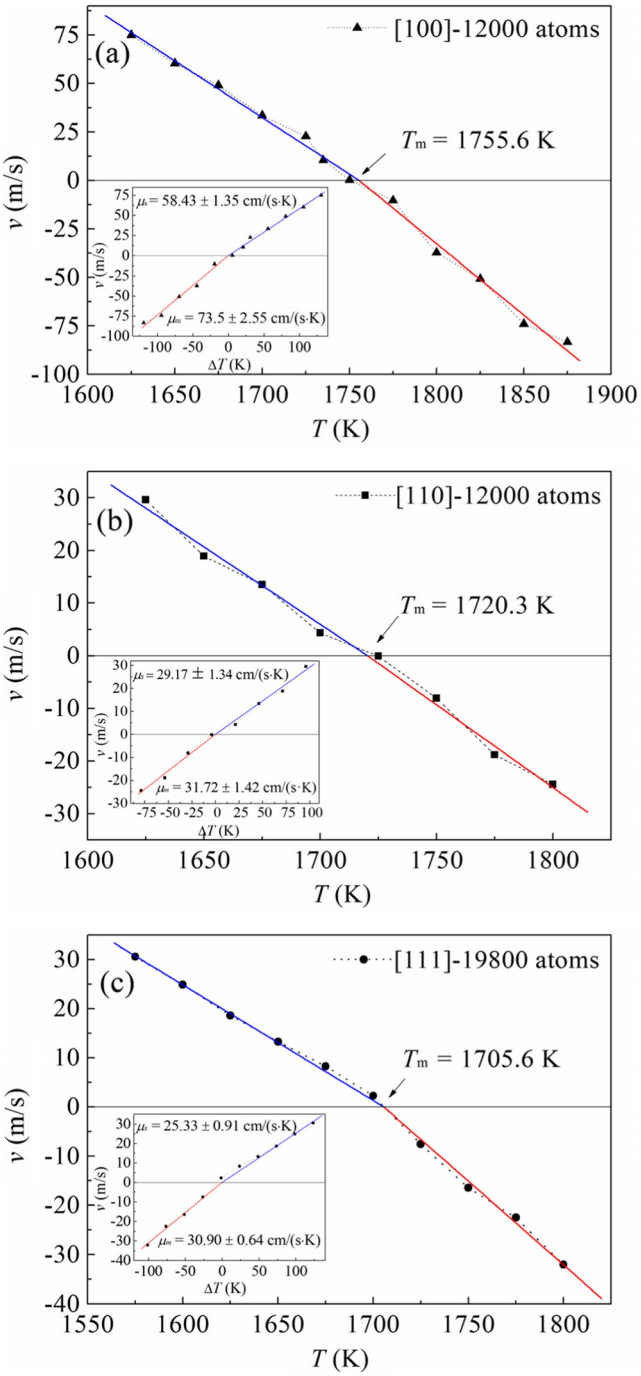

Fig. 5 Velocities of *s*-*l* interfaces as a function of *T* for systems of [100], [110], and [111] orientations containing 12,000, 12,000, and 19,800 atoms. The melting temperatures T_ms, corresponding to the intersections where the interfacial velocities are zero, were achieved by linear fitting both sets of the positive and negative data simultaneously with a restriction of the same *x* intercept; the insets show the relationships between velocities and ΔTs. The kinetic coefficients μ_ss and μ_ms were linear fitting slopes of positive and negative data points, separately

T_ms of Al, Cu, and Ni with EAM potentials also showed high coincidence to CPM results [38]. IVM results proved the reasonability of CPM, and further the precise dependence between pressure and temperature in the coexisting systems with NVE ensemble. This conformity also suggests that the ensemble switching from NVE to NPT affects very slightly on the values of T_ms.

According to the definition of kinetic coefficient μ in Eq. (1), the slopes of the fitting lines between v and ΔT, defined respectively as μ_s and μ_m, were calculated. The subscripts s and m were set to distinguish the solidifying and

melting processes. Hence, the ratio of μ_m/μ_s reflects the degree of asymmetry. The last four columns in Table 1 show the values of μ for different interface orientations and system sizes. Some literature results [10, 18] for BCC Fe are also listed for comparisons. We can find clearly that μ fluctuates at a certain extent with the orientations and sizes. Comparing the three orientations with each other, [100] have the largest values of $\mu_{s,[100]}$=59.42 cm/(s·K) (group mean values of the three different sizes), while $\mu_{s,[110]}$=31.33 cm/(s·K) and $\mu_{s,[111]}$=27.14 cm/(s·K). The main trend of $\mu_{s,[100]} >> \mu_{s,[110]} > \mu_{s,[111]}$ is similar to Sun et al.'s [18] and Watanabe et al.'s [21] consequences for BCC Fe. However, the values of $\mu_{s,[100]}$ we got are larger than both Sun et al.'s [18] result (45.8±3.8 cm/(s·K)) and Watanabe et al.'s result (30.5 cm/(s·K)), although the values of $\mu_{s,[110]}$ and $\mu_{s,[111]}$ agree very well with Sun et al.'s [18]. Therefore, the ratios $\mu_{s,[100]}/\mu_{s,[110]} \sim \mu_{s,[100]}/\mu_{s,[111]} \sim 2.2\pm0.5$ were larger than their result ~1.35. That means, [100] orientation of BCC Fe expresses larger moving tendency in our experiments. Those differences could be ascribed partially to the different potential functions. As BGJ model predicts, $\mu_{[110]}$ should be largest in BCC system, because $d_{[110]}$ ($\sqrt{2}a/2$) is larger than $d_{[100]}$ ($a/2$) and $d_{[111]}$ ($\sim\sqrt{3}a/4$). So, BGJ model is also not suitable for all the results of BCC system. Celestini and Debierre [19] found the existence of the size effect on μ in their MD research on pure Au. They argued that μ is smaller for a system with larger cross sectional area, especially for [111] orientations. They thought a large system will waste more solidification driving forces to rearrange the interfacial microstructure so that the interfacial velocities are lower for large systems. However, just on the contrary, we found μ is larger when the system has larger cross sectional area, through the self-comparison in both [100] and [111] orientation groups. Hoyt and Asta's [16] results also showed system size effect on [111] orientation that smaller system size possesses roughly 50 % higher growth rate than large system. However, it was not confirmed for the [100] and [110] orientations. Our kinetic coefficients show about 10–28 % variations with systems sizes. Unfortunately, we did not find distinct dependent relationship on the length of Z axis. We tend to consider the discrepancies of different systems come from the statistical uncertainties. We cannot decide yet how much of this result relates to the potential and the statistical uncertainties. Maybe, there is a need for more precise contrastive experiments to be further studied.

As another discovery, asymmetries between solidifying and melting similar to Celestini and Debierre's research on Au [19] are also found here. Firstly, the values of μ_ms are all larger than μ_ss for systems with different orientations and sizes. This result agrees very well with the former descriptions about asymmetry that melting is faster than solidifying [19, 39]. Tsao et al. [39] also argued that melting of silicon was inherently faster than solidifying at the same temperature deviations in laser-induced zone melting experiments. Tymczak and Ray's [37] simulations on BCC Na also found a clear slope discontinuity between melting and solidifying. In our works, ratio of μ_m/μ_s was calculated as a parameter to describe the asymmetry. We find that the ratios of μ_m/μ_s fluctuate slightly with orientations and system sizes but all exceed 1, which means that all μ_ms are larger than corresponding μ_ss. Here, we use the mean value of the three different systems along the same orientation to describe the asymmetry. As a result, $\mu_m/\mu_s|_{[100]} \sim 1.25$, $\mu_m/\mu_s|_{[110]} \sim 1.13$, and $\mu_m/\mu_s|_{[111]} \sim 1.43$. So, [111] orientation has the largest ratio while [110] value is the smallest. Interestingly, this conclusion was in reasonable agreement with Celestini and Debierre's conclusions [19] on FCC Au although they have different structures. Even so, in our works asymmetries values are not as large as their results ($\mu_m/\mu_s|_{[100]} \sim 2.1$, $\mu_m/\mu_s|_{[110]} \sim 1.6$, and $\mu_m/\mu_s|_{[111]} \sim 3.6$) [19]. This feature of results is discrepant with Sun et al.'s conclusions on BCC Fe [40] and FCC Ni [10]. They obtained highly symmetric results for melting and solidifying kinetics in the regime of low supercoolings (ΔT<40 K in their works). Additionally they argued that the discrepancies with Celestini and Debierre's Au simulations ($\Delta T \sim 200$ K) were caused by the different interatomic potentials and thermal gradients [10]. In our experiments, the values of ΔTs>100 K were much larger than Sun et al.'s ΔT but much lower than Celestini and Debierre's ΔT. As we deduced, the temperature deviation magnitude ΔT may be the major cause for the contradiction between our works and Sun et al.'s results on BCC Fe. Also, the different fitting scheme enlarges this contradiction a lot. Especially, Tepper and Briels [41] concluded that asymmetry between melting and solidifying rates around equilibrium temperature was also caused by the different starting configurations for melting and solidifying processes, and imperfections were evolved in solidifying process, but were absent in melting process. Oppositely, all our melting and solidifying simulations were started from the same NVE equilibrated configuration, asymmetry still arose. Therefore, we do not think the different initial configurations are the intrinsic cause for the asymmetry. Finally, we find the order, $\mu_{m,[100]} >> \mu_{m,[111]} > \mu_{m,[110]}$, for BCC Fe during melting processes. Celestini and Debierre's results on FCC Au show a similar anisotropy ($\mu_{m,[100]} > \mu_{m,[111]} > \mu_{m,[110]}$) [19].

Interfacial roughness

In this section, a searching method for identifying interfacial atoms is briefly introduced. With this searching procedure we precisely located the interface and

calculated a parameter defined in Eq. (4) to describe the interfacial roughness.

$$R_{\mathrm{int}} = \sqrt{\frac{\sum_{1}^{n_{\mathrm{int}}} \left(z_{\mathrm{int},i} - \overline{z_{\mathrm{int}}}\right)^2}{n_{\mathrm{int}}}} \tag{4}$$

Where, n_{int} is the total number of interfacial atoms; $Z_{\mathrm{int},i}$ means the Z coordinate of interfacial atom i. $\overline{Z_{\mathrm{int},i}}$ denotes the average Z coordinate of all interfacial atoms. Based on the similar principle, another parameter S/S_0 was also used to describe the ratio of realistic interfacial area (S) to ideal flat cross-sectional area (S_0).

Previously, we introduced ABOO+VP method to strictly determine solid or liquid atoms. Based on this determination, we further define those solid atoms, around which there are some liquid atoms within their nearest neighbors [28], as interfacial atoms. We can also define the liquid atoms with some solid nearest neighbors as interfacial atoms. There is no difference between these two choices for the precise determination of interface and we just chose the former. However,, this definition is far from the precise localization of the interface because of the great number of spontaneous "solid-like" atoms in the liquid part and "liquid-like" atoms in the solid body due to the thermal motion. Therefore, we introduced a searching method to precisely locate the interface. Here is just a brief description of the searching method and the detailed description will be presented somewhere else. In this method, we proved that, for any interfacial atoms in the real interface, their nearest neighbors must contain some other interfacial atoms. That means the whole interface should be formed with the interfacial atoms one-by-one neighboring with each other. So, if we can locate any one atom of the interface, we can locate the whole interface through the nearest neighbor searching scheme. Based on this definition and the interface searching method, two independent and continuous interfaces (in Fig. 6 (a)) were found out in each coexisting system. Figure 6 (b) is the corresponding 3D contour map of interface 2 in Fig. 6 (a). The realistic interfacial area mentioned above is area integration of this 3D contour surface. The protuberant areas could be atoms growing faster than average interfacial atoms at that moment. It is a clear multiple growth phenomenon (growing simultaneously at multiple sites, instead of a single two-dimensional island) [42] of a rough *s-l* interface. When comparing several 3D interfacial surfaces of [100], [110], and [111] orientations, we can not definitely conclude that [100] interfaces are rougher than the other two orientations (as we expect to find out why [100] orientations have the largest kinetic coefficients, and generally, rougher interface grows faster under the same undercooling). Additionally we

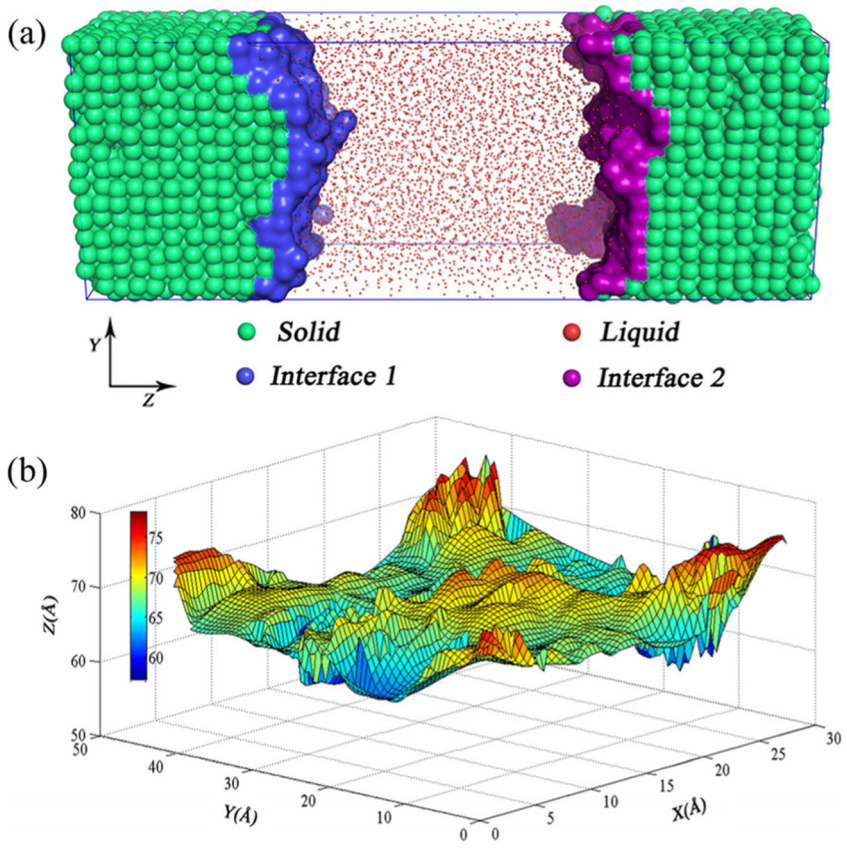

Fig. 6 Snapshot of [100] coexisting system with solid, liquid, and interfacial atoms, where solid atom is represented as green ball, liquid atom is red dot, as well as the blue surface for interface 1 and the purple surface for interface 2 (**a**); 3D contour map of interface 2 (**b**). The multiple growth phenomenon of rough *s-l* interface is proposed from this map

can not find the magnitude order of interfacial roughness among these three orientations just through the sense of 3D sight.

Three independent coexisting systems with [100], [110], and [111] orientations respectively (three systems shown in Fig. 4) were put into "cryostats" (or "pyrostats") with 25 K and 100 K temperature deviations. They were all solidified (or melted) and the *s-l* interfaces moved forward (or back). Finally, we made statistical analysis on R_{int} and S/S_0 within the smooth and steady solidifying and melting processes of the 12 systems (3 samples×4 temperature deviations). Figure 7 is taking the R_{int} and S/S_0 for [100] oriented system with 12,000 atoms as an example, calculated from 2000 to 12,000 steps (from 4 ps to 24 ps) with 50 steps interval at 1660.7 K (ΔT=100 K). We can see that the roughness R_{int} varies between 2 and 5.5 and the ratio of S/S_0 varies between 1.3 and 3. All statistical average data are grouped into four items and listed in Table 2. Items *A* to *D* are systems with temperature deviations of 25 K and 100 K, respectively. From an overall perspective, R_{int} and S/S_0 increase with the temperature regardless of the melting or solidifying processes. R_{int} and S/S_0 with 100 K superheating are all bigger than other items. After observing the melting snapshots, we find the solid phase collapses faster under 100 K superheating, but it is not obvious under 25 K superheating. That is why the interfacial fluctuations of item *D* are larger than item *C*'s. However, when it comes to solidifying processes, this explanation is inadequate: item *A*, with large ΔT (100 K), finally show smaller fluctuations than item *B* with 25 K supercooling. Maybe, the latent heat of crystallization with 100 K supercooling did not have enough time to diffuse as a system with 25 K supercooling, and the accumulative latent heat restrained the growing of protruding solid front. Comparing the three orientations of every item, [100] shows larger S/S_0 than [110] and [111]. This result is identical to the former kinetic coefficient orders, $\mu_{[100]} >> \mu_{[110]}, \mu_{[111]}$. It is evident that [100] interfaces are rougher than the other two orientations. Furthermore, including R_{int}s, these two parameters for [110] are smallest in all items. This is in accordance with melting kinetics that $\mu_{m,[100]} >> \mu_{m,[111]} > \mu_{m,[110]}$. As a conclusion, the roughness anisotropies are approximately [100]>[111]>[110]. Buta et al. [24] also found the interface structural anisotropy in simulations on silicon: interface width was 0.681±0.001 nm for [111], larger than 0.570±0.005 nm for [100]. However, their analysis objects were equilibrium interfaces under NVE conditions. Huitema et al. [26] measured the growing *s-l* interface of Lennard-Jones under 12 K supercooling and found the widths were 0.63 nm for [100] and 0.80 nm for [110] and [111] interfaces. Although the interface width is not strictly defined as a concept of interfacial roughness, it still demonstrates the existence of the interface structural anisotropy.

Table 2 Comparisons of the interfacial roughness R_{int} and area ratio S/S_0 statistical data for three different orientations under 25 K and 100 K temperature deviations, ΔT

Item	Orientation	T_m (K)	ΔT (K)	T (K)	R_{int} (Å)	S/S_0
A	100	1760.7	100	1660.7	3.066	1.845
	110	1718.7		1618.7	2.932	1.744
	111	1705.6		1605.6	3.197	1.761
B	100	1760.7	25	1735.7	3.507	2.075
	110	1718.7		1693.7	3.240	1.932
	111	1705.6		1680.6	3.340	1.927
C	100	1760.7	-25	1785.7	3.364	2.095
	110	1718.7		1743.7	3.118	1.901
	111	1705.6		1730.6	3.367	1.944
D	100	1760.7	-100	1860.7	4.014	2.467
	110	1718.7		1818.7	3.453	2.149
	111	1705.6		1805.6	3.800	2.284

When comparing items with the same temperature deviations (*B* with *C*, *A* with *D*), the roughness disparities along the same orientations between *B* and *C* ($|(R_{int})_s-(R_{int})_m|_{\Delta T=25K}$:

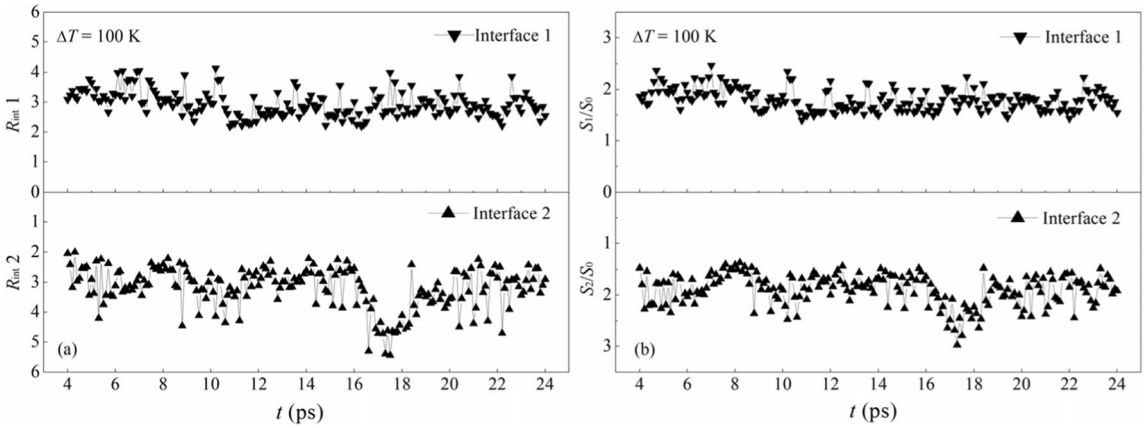

Fig. 7 Variation of the interfacial roughness R_{int} and ratios of S/S_0 for two interfaces of [100] orientation with 100 K supercooling (T=1660.7 K) calculated from 4 to 24 ps at 0.1 ps intervals

0.027~0.143 and $|(S/S_0)_s\text{-}(S/S_0)_m|_{\Delta T=25K}$: 0.02~0.031) are much weaker than A and D ($|(R_{int})_s\text{-}(R_{int})_m|_{\Delta T=100K}$: 0.521~0.948 and $|(S/S_0)_s\text{-}(S/S_0)_m|_{\Delta T=100K}$: 0.405~0.622). This is evidence for why asymmetry between melting and solidifying is obvious in large temperature deviations. Also, this can be a reasonable explanation for why Sun et al.'s results are different from Celestini and Debierre's results in Au. In our experiment, ΔT locates between Sun et al.'s and Celestini and Debierre's ΔTs, and we also find the medium asymmetry. Therefore, we can conclude that the farther the temperature deviates from the equilibrium melting point, the stronger the asymmetry is between the corresponded solidifying and melting rates.

Conclusions

In this paper, MD simulation was used to calculate melting temperature T_m and kinetic coefficient μ of BCC Fe with Sutton-Chen potential in order to explore the anisotropy between crystal orientations and asymmetry between melting and solidifying processes. Using CPM, the melting point T_m was calculated for three low index orientations [100], [110], and [111]. As a consequence, $T_{m,[100]}$s are larger than $T_{m,[110]}$s and $T_{m,[111]}$s. The decreasing ranges are about 20~40 K from [100] to [110] and continuously to [111]. IVM results accord well with CPM results despite some acceptable slight deviations (<7 K). IVM results proved the reasonability of CPM, and further the precise dependence between pressure and temperature in the coexisting systems with NVE ensemble.

To explore the anisotropy of the *s-l* interface, the kinetic coefficient μ was calculated by putting NVE coexisting systems (with different orientations and different sizes) into supercooling/superheating baths. μ was separated into μ_s and μ_m to investigate the asymmetry of solidifying and melting kinetics. Compared with Sun et al.'s results ($\mu_{[100]}>\mu_{[110]}\sim\mu_{[111]}$), similar conclusions, $\mu_{s,[100]} >> \mu_{s,[110]} > \mu_{s,[111]}$, $\mu_{m,[100]} >> \mu_{m,[111]} > \mu_{m,[110]}$, were obtained. However, we obtained larger values of $\mu_{[100]}$s (about 67 cm/(s·K)).

At last, two parameters, interfacial roughness R_{int} and area ratio S/S_0, were introduced to describe the interfacial structure anisotropies of three orientations in melting and solidifying processes. With the help of the interface searching method, interfacial roughness anisotropies were found approximately as [100]>[111]>[110]. Evidence shows that [100] interfaces are rougher than the other two orientations. That is also one reason why $\mu_{[100]}>\mu_{[110]}\sim\mu_{[111]}$. As another important discovery, asymmetry of roughness is larger when temperature deviation is larger. This is an explanation for the asymmetry discrepancies between Sun et al.'s, Celestini and Debierre's and our results. In our experiment, ΔT (~100 K) locates between their ΔTs (~40 K and ~200 K), and we also find medium asymmetry between Sun et al.'s and Celestini and Debierre's.

Acknowledgments This work is supported by National Natural Science Foundation of China (Nos. 50504010, 50974083, 51174131, 51374141), Joint Funds of the National Natural Science Foundation of China (No. 50774112), National Basic Research Program of China (No. 2012CB722805).

References

1. Burke E, Broughton JQ, Gilmer GH (1988) Crystallization of fcc (111) and (100) crystal-melt interfaces: a comparison by molecular dynamics for the Lennard-Jones system. J Chem Phys 89(2):1030–1041. doi:10.1063/1.455254
2. Davidchack RL, Laird BB (1998) Simulation of the hard-sphere crystal–melt interface. J Chem Phys 108(22):9452–9462. doi:10.1063/1.476396
3. Morris JR (2002) Complete mapping of the anisotropic free energy of the crystal-melt interface in Al. Phys Rev B 66(14):144104. doi:10.1103/PhysRevB.66.144104
4. Liu YH, Wu YQ, Shen T, Wang ZK, Jiang GC (2010) Molecular dynamics simulation of phase transformation of γ-Fe→δ-Fe→liquid Fe in continuous temperature rise process. Acta Metall Sin 46(2):172–178
5. Dinsdale AT (1991) SGTE data for pure elements. Calphad 15(4):317–425. doi:10.1016/0364-5916(91)90030-N
6. Luo SN, Strachan A, Swift DC (2004) Nonequilibrium melting and crystallization of a model Lennard-Jones system. J Chem Phys 120(24):11640–11649. doi:10.1063/1.1755655
7. Shen T, Meng WJ, Wu YQ, Lu XG (2013) Size dependence and phase transition during melting of fcc-Fe nanoparticles: a molecular dynamics simulation. Appl Surf Sci 277:7–14. doi:10.1016/j.apsusc.2013.03.017
8. Shibuta Y, Takamoto S, Suzuki T (2008) A molecular dynamics study of the energy and structure of the symmetric tilt boundary of iron. ISIJ Int 48(11):1582–1591. doi:10.2355/isijinternational.48.1582
9. Morris JR, Wang CZ, Ho KM, Chan CT (1994) Melting line of aluminum from simulations of coexisting phases. Phys Rev B 49(5):3109–3115. doi:10.1103/PhysRevB.49.3109
10. Sun DY, Asta M, Hoyt JJ (2004) Kinetic coefficient of Ni solid–liquid interfaces from molecular-dynamics simulations. Phys Rev B 69(2):024108. doi:10.1103/PhysRevB.69.024108
11. Ackland GJ, Bacon DJ, Calder AF, Harry T (1997) Computer simulation of point defect properties in dilute Fe-Cu alloy using a many-body interatomic potential. Philos Mag A 75(3):713–732. doi:10.1080/01418619708207198
12. Mendelev MI, Han S, Srolovitz DJ, Ackland GJ, Sun DY, Asta M (2003) Development of new interatomic potentials appropriate for crystalline and liquid iron. Philos Mag 83(35):3977–3994. doi:10.1080/14786430310001613264
13. Foiles SM, Adams JB (1989) Thermodynamic properties of fcc transition metals as calculated with the embedded-atom method. Phys Rev B 40(9):5909–5915. doi:10.1103/PhysRevB.40.5909
14. Sutton AP, Chen J (1990) Long-range Finnis–Sinclair potentials. Philos Mag Lett 61(3):139–146. doi:10.1080/09500839008206493
15. Broughton JQ, Gilmer GH, Jackson KA (1982) Crystallization rates of a Lennard-Jones liquid. Phys Rev Lett 49(20):1496–1500. doi:10.1103/PhysRevLett.49.1496

16. Hoyt JJ, Asta M (2002) Atomistic computation of liquid diffusivity, solid–liquid interfacial free energy, and kinetic coefficient in Au and Ag. Phys Rev B 65(21):214106. doi:10.1103/PhysRevB.65.214106
17. Hoyt JJ, Sadigh B, Asta M, Foiles SM (1999) Kinetic phase field parameters for the Cu–Ni system derived from atomistic computations. Acta Mater 47(11):3181–3187. doi:10.1016/S1359-6454(99)00189-5
18. Sun DY, Asta M, Hoyt JJ (2004) Crystal-melt interfacial free energies and mobilities in fcc and bcc Fe. Phys Rev B 69(17):174103. doi:10.1103/PhysRevB.69.174103
19. Celestini F, Debierre J-M (2002) Measuring kinetic coefficients by molecular dynamics simulation of zone melting. Phys Rev E 65(4):041605. doi:10.1103/PhysRevE.65.041605
20. Hoyt JJ, Asta M, Sun DY (2006) Molecular dynamics simulations of the crystal–melt interfacial free energy and mobility in Mo and V. Philos Mag 86(24):3651–3664. doi:10.1080/14786430500156625
21. Watanabe Y, Shibuta Y, Suzuki T (2010) A molecular dynamics study of thermodynamic and kinetic properties of Solid–liquid interface for Bcc iron. ISIJ Int 50(8):1158–1164
22. Finnis MW, Sinclair JE (1984) A simple empirical N-body potential for transition metals. Philos Mag A 50(1):45–55. doi:10.1080/01418618408244210
23. Morris JR, Song X (2003) The anisotropic free energy of the Lennard-Jones crystal-melt interface. J Chem Phys 119(7):3920–3925. doi:10.1063/1.1591725
24. Buta D, Asta M, Hoyt JJ (2008) Atomistic simulation study of the structure and dynamics of a faceted crystal-melt interface. Phys Rev E 78(3):031605. doi:10.1103/PhysRevE.78.031605
25. Broughton JQ, Bonissent A, Abraham FF (1981) The fcc (111) and (100) crystal–melt interfaces: a comparison by molecular dynamics simulation. J Chem Phys 74(7):4029–4039. doi:10.1063/1.441583
26. Huitema H, Vlot M, Van der Eerden J (1999) Simulations of crystal growth from Lennard-Jones melt: detailed measurements of the interface structure. J Chem Phys 111:4714–4723. doi:10.1063/1.479233
27. Jesson BJ, Madden PA (2000) Structure and dynamics at the aluminum solid–liquid interface: an ab initio simulation. J Chem Phys 113(14):5935–5946. doi:10.1063/1.1290702
28. Li R, Wu YQ, Xiao JJ (2014) The nucleation process and the roles of structure and density fluctuations in supercooled liquid Fe. J Chem Phys 140(3):034503. doi:10.1063/1.4861587
29. Smith W, Forester TR (1996) DL_POLY_2.0: a general-purpose parallel molecular dynamics simulation package. J Mol Graph 14(3):136–141. doi:10.1016/S0263-7855(96)00043-4
30. Smith W, Yong CW, Rodger PM (2002) DL_POLY: application to molecular simulation. Mol Simul 28(5):385–471. doi:10.1080/08927020290018769
31. Smith W, Todorov IT (2006) A short description of DL_POLY. Mol Simul 32(12–13):935–943. doi:10.1080/08927020600939830
32. Berendsen HJC, Postma JPM, van Gunsteren WF, DiNola A, Haak JR (1984) Molecular dynamics with coupling to an external bath. J Chem Phys 81(8):3684–3690. doi:10.1063/1.448118
33. Lechner W, Dellago C (2008) Accurate determination of crystal structures based on averaged local bond order parameters. J Chem Phys 129:114707. doi:10.1063/1.2977970
34. Rycroft CH (2009) VORO++: a three-dimensional Voronoi cell library in C++. Interdiscip J Nonlinear Sci 19(4):041111. doi:10.1063/1.3215722
35. Shibuta Y, Suzuki T (2007) Melting and nucleation of iron nanoparticles: a molecular dynamics study. Chem Phys Lett 445(4–6):265–270. doi:10.1016/j.cplett.2007.07.098
36. Sorkin V, Polturak E, Adler J (2003) Molecular dynamics study of melting of the bcc metal vanadium. II. Thermodynamic melting. Phys Rev B 68(17):174103. doi:10.1103/PhysRevB.68.174103
37. Tymczak CJ, Ray JR (1990) Asymmetric crystallization and melting kinetics in sodium: a molecular-dynamics study. Phys Rev Lett 64(11):1278–1281. doi:10.1103/PhysRevLett.64.1278
38. Mendelev M, Rahman M, Hoyt J, Asta M (2010) Molecular-dynamics study of solid–liquid interface migration in fcc metals. Model Simul Mater Sci Eng 18(7):074002. doi:10.1088/0965-0393/18/7/074002
39. Tsao JY, Aziz MJ, Thompson MO, Peercy PS (1986) Asymmetric melting and freezing kinetics in silicon. Phys Rev Lett 56(25):2712–2715. doi:10.1103/PhysRevLett.56.2712
40. Sun DY, Asta M, Hoyt JJ, Mendelev MI, Srolovitz DJ (2004) Crystal-melt interfacial free energies in metals: fcc versus bcc. Phys Rev B 69(2):020102. doi:10.1103/PhysRevB.69.020102
41. Tepper H, Briels W (2001) Simulations of crystallization and melting of the FCC (100) interface: the crucial role of lattice imperfections. J Cryst Growth 230(1):270–276. doi:10.1016/S0022-0248(01)01339-2
42. Ryu S, Cai W (2011) Molecular dynamics simulations of gold-catalyzed growth of silicon bulk crystals and nanowires. J Mater Res 26(17):2199–2206. doi:10.1557/jmr.2011.155